

Uncontrolled Generation of Traciton Motors in Hybrid Electric Vehicles

Xiaofeng Ding¹, Jinglin Liu², and Chris Mi³

¹ Department of Electrical Engineering, Northwestern Polytechnical University, dx_f_219@163.com

² Department of Electrical Engineering, Northwestern Polytechnical University, JinglinL@nwpu.edu.cn

³ Department of Electrical and Computer Engineering, University of Michigan-Dearborn, mi@jeee.org

Abstract

Interior permanent magnet synchronous motor (IPMSM) systems are vulnerable to uncontrolled generation (UCG) when the inverter switches loss their drive signals suddenly during flied weakening high speed operation. At this point, uncontrolled rectifier is composed by freewheel diodes in the inverter, the current comes from the motor through the rectifier, and then charges the battery. This paper develops a simple analytical model of this system firstly, and then carries out the simulation of UCG transient process to investigate the impact of the motor speed, battery capacity and other factors on UCG and feedback-power obtained throughout the process. Moreover, circuit improvement is presented in order to avoid destruction risk of the battery, motor, inverter and other relevant components during UCG.

Keywords

interior permanent magnet synchronous motor, uncontrolled generation, rectifier, flied weakening, feedback-power

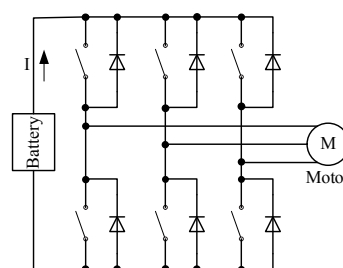
1. INTRODUCTION

Permanent magnet synchronous machines (PMSM) are provided with advantages of small size, light weight, and high power density, therefore PMSM are primary choice as traction motors in hybrid vehicles. In addition, with the development of power electronics, motor control technologies are further improved. And the motor speed range is expanded due to the improvement of the field weakening speed regulation. For this reason, more and more hybrid vehicles use PMSM [Kassakian, 2000].

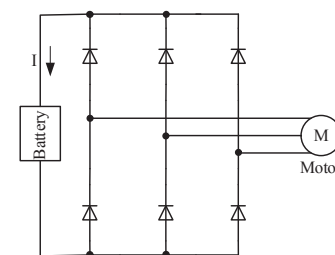
However, interior permanent magnet synchronous motor (IPMSM) systems are vulnerable to uncontrolled generation (UCG) when the inverter switches loss their drive signals suddenly during flied weakening high speed operation [Bianchi et al., 1996; Jahns and Caliskan, 1999; Liaw et al., 2000, 2005; Soong and Ertugrul, 2004; Adnanes et al., 1992.]. The typical electrical powertrain in the hybrid vehicles is shown in Fig. 1a, including battery, inverter and motor. And the motor with high speed is assumed. At this point, the drive signals of inverter switches disappear and the equivalent back electromotive force (EMF) of the motor is higher than the voltage of the battery. As a result, freewheel diodes in the inverter form uncontrolled rectifier inverter as shown in Figure 1 (b). The current induced by back EMF will flow through the freewheel diodes, and then charge the battery. And it

will disappear until the equivalent back EMF is equal to the voltage of the battery.

This paper presents a simple analytical model of this system firstly, and then implements the simulation of UCG transient process to investigate the impact of the motor speed, battery capacity and other factors on UCG. And feedback-power is estimated throughout the process. Moreover, a leakage resistance is added to the circuit in order to protect the battery, motor, inverter and other relevant components during UCG.



(a) Inverter operation



(b) UCG operation

Fig. 1 IPMSM and drive system

2. SIMPLE ANALYTICAL MODEL OF UCG

2.1 Model of the battery

The equivalent circuit of the battery is depicted in Figure 2, the output voltage of the battery is sum of no load voltage and voltage-drop on the resistance, therefore, the mathematical model of the battery voltage is derived as, Eq (1).

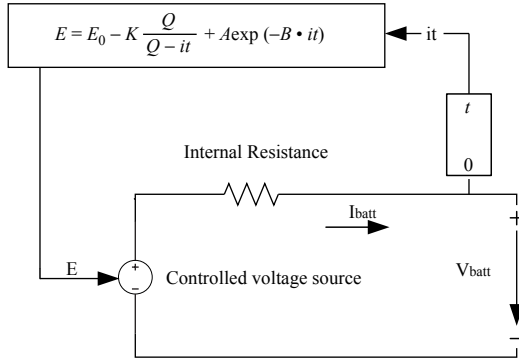


Fig. 2 Equivalent circuit of battery

$$V_{batt} = E - R \cdot I_{batt} \\ = E_0 - K \frac{Q}{Q - it} + Ae^{(-B \cdot it)} - R \cdot I_{batt} \quad (1)$$

Where,

- E , no load voltage
- E_0 , constant voltage
- K , polarization voltage
- Q , battery capacity
- A , exponential voltage
- B , exponential capacity

2.2 Model of uncontrolled rectifier

The inverter turns into a rectifier due to all switches are turned off during UCG process. Therefore, the mathematic equation is given in Eq. (2).

$$V = \frac{3\sqrt{2}}{\pi} V_{L-L,rms} \cos \alpha \\ = 1.35V_{L-L,rms} \quad (2)$$

Where,

- V , output DC voltage of rectifier;
- $V_{L-L,rms}$, line-line voltage effective value of motor;
- α , conduction angles of switch, the value is 0 for diode

2.3 Model of motor

According to the analyzing issue, two assumptions are set:

- (1) The output voltage of the motor is proportional to motor speed;
- (2) The speed variation rate is constant.

Consequently, the model of the motor is written in Eq.

(3).

$$V_{L-L,rms} = K\omega(1 - \alpha t) \quad (3)$$

Where,

- ω , motor speed;
- K , voltage constant;
- α , speed variation rate.

2.4 Model of the system

The output voltage of the rectifier is obtained from Eq (2), Eq (3) as shown in Eq. (4).

$$V = 1.35K\omega(1 - \alpha t) \quad (4)$$

Therefore, the model of UCG system is formed by Figure 3 shows the process of UCG, curves 1 and 4 represent the equation 1 and equation 4 respectively. The output voltage of rectifier V_0 is higher than the battery voltage V_1 at the beginning of UCG. With the decline in motor speed, the rectifier output voltage is gradually reduced. Meanwhile, the battery voltage is increased slowly through the continuous charging current. Than the current will gradually disappear when the battery voltage equal to the voltage of the rectifier at t_1 . In the end, the battery voltage maintain the constant value V_2 and the rectifier output voltage will drop to 0 as the motor speed down.

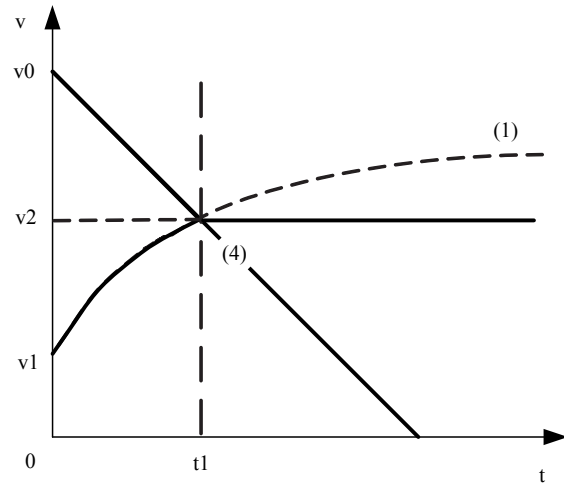


Fig. 3 Uncontrolled generation

3. SIMULATION OF UCG TRANSIENT PROCESS

3.1 Simulation model and results

Figure 4 describes IPMSM and its drive system developed in Simulink, including motor, inverter and battery. The motor and battery parameters are shown in Table 1 and Table 2. The voltage constant of the motor represents per 1000 rpm produces 82.4 V peak line to

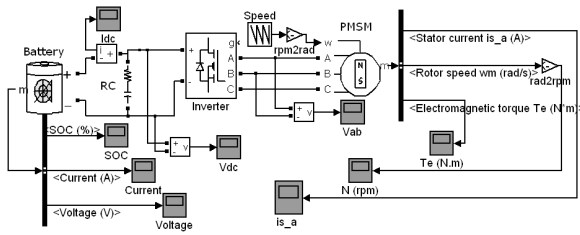


Fig. 4 Simulation model of UCG

Table 1 Parameters of IPMSM

Rated power (kW)	35
Rated speed (rpm)	3000
d-axis inductance (mH)	6.5
q-axis inductance (mH)	13.5
Voltage constant (V_peak L-L/krpm)	82.4677
Pole pairs	4
Phase resistance of winding (Ω)	0.05

Table 2 Parameters of battery

Type	lithium-ion
Rated voltage (V)	200
Rated capacity (Ah)	6.5
State of charge (%)	100

line voltage in the motor. Lithium-ion batteries have higher energy density, greatly reducing the weight of the battery pack. In addition, lithium-ion batteries possess low self-discharge, long cycle life, no memory effect and environmental-friendly characteristics etc. Therefore, the batteries are applied to more and more hybrid vehicles.

Figure 5 depicts the overall process of UCG, there are motor speed, DC side current of rectifier and line voltage of motor individually from top to bottom. The motor speed slows down from 5000 rpm to 0 rpm. And the current disappears around 0.43 seconds, which represents the rectifier shut down totally. Then the line to line voltage decreases with the speed descending gradually, and both of them drop to 0 in the end.

The parts of the line voltage V_{ab} around 0.3 s and 0.4 s in Figure 5 are enlarged, as shown on Figure 6 (a) and Figure 6 (b). The six step waveform of the line to line voltage changes into sine waveform smoothly during the UCG process. The six step is due to the battery connected to the DC side of the rectifier, and the sine waveform is the no load back EMF of the motor after the rectifier is turned off.

Figure 7 shows the transition of the battery state of

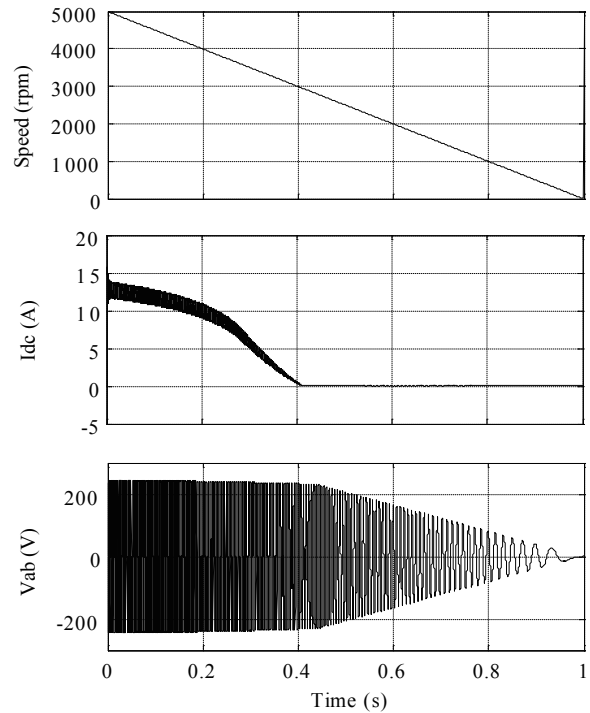
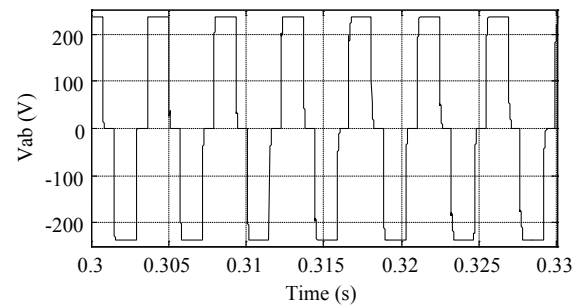
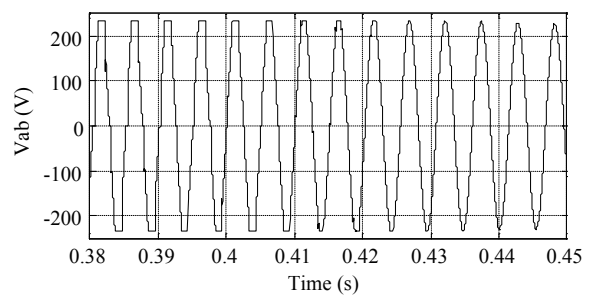


Fig. 5 Motor speed, DC voltage of rectifier and line voltage of motor



(a) Range of 0.3-0.33 s



(b) Range of 0.18-0.45 s

Fig. 6 Motor line voltage

charge (SOC), current and voltage respectively from top to bottom during the UCG. The negative current of battery represents charging the battery. The SOC ascends from 100 % to 100.014 %. The small increment is owing to the charging time is relatively short. In addition, the output voltage of battery is sum of no load voltage and voltage-drop on internal resistance

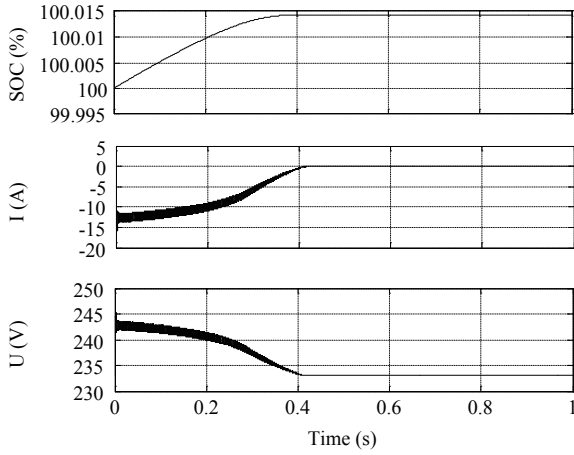


Fig. 7 SOC, current and output voltage of battery under capacity of 6.5 Ah

as known from expression 1. Then the output voltage is equal to the no load voltage when the current disappears. Therefore, the output voltage of battery decreases firstly and then maintains a constant value after 0.43s.

In order to calculate the feedback power from the battery, the product of the current and output voltage of the battery is integrated. And the estimation value is 850J, as shown in Figure 8. The feedback power holds a constant value after 0.43 s due to the disappearance of the current as well as the output voltage of the battery.

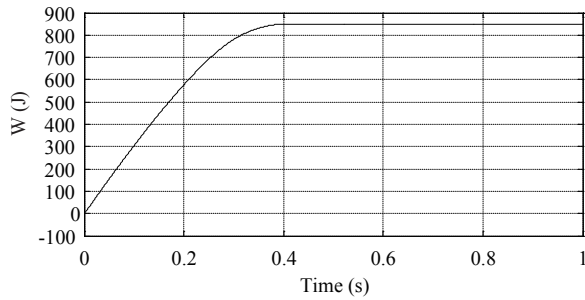
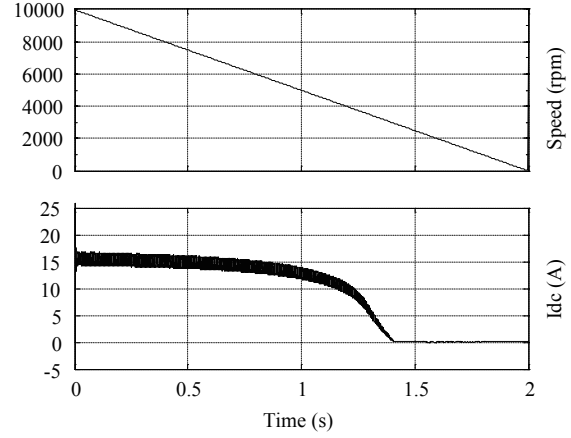


Fig. 8 Absorbed energy of battery

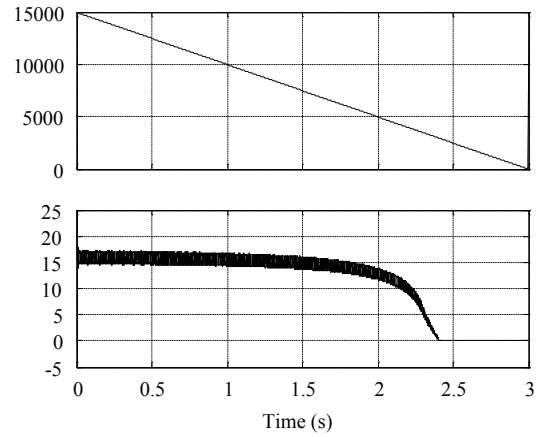
3.2 Effect of motor speed on UCG

Two UCG simulations with motor speed range of 10000-0 rpm and 15000-0 rpm were carried out, as shown in Figure 9 (a) and Figure 9 (b) respectively. Although the speed increases dramatically, the current increment is tiny. This interesting phenomenon is due to the current tends to a constant value during UCG. The constant value is determined by flux and d-axis inductance [Jahns and Caliskan, 1999].

The steady-state d-axis and q-axis are given, as follows [Jahns and Caliskan, 1999],



(a) 10000-0 rpm



(b) 15000-0 rpm

Fig. 9 Two UCG with different high speed

$$V_{qn} = \omega_n \Psi_{mn} + \omega_n L_{dn} I_{dn} \tag{5}$$

$$V_{dn} = -\omega_n L_{qn} I_{qn} \tag{6}$$

where,

V_{dn} , d-axis voltage;

V_{qn} , q-axis voltage;

L_{dn} , d-axis inductance;

L_{qn} , q-axis inductance;

I_{dn} , d-axis current,

I_{qn} , q-axis current,

ω_n , motor velocity;

Ψ_{mn} , flux linkage;

where subscript n signifies unit value and uppercase variables signify steady-state values.

The phasor diagram shown in Figure 10 corresponds to an IPM machine in the synchronously rotating reference frame operating in the UCG mode, than the components of V_{sn} and I_{sn} can be expressed as follows:

$$I_{dn} = -I_{sn} \sin \gamma \quad V_{dn} = V_{sn} \sin \gamma \tag{7}$$

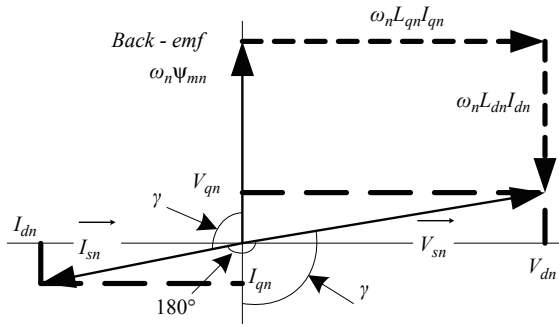


Fig. 10 Phasor diagram of IPMSM during UCG operation

$$I_{qn} = I_{sn} \cos \gamma \quad V_{qn} = -V_{sn} \cos \gamma \quad (8)$$

The expressions for V_{dn} and I_{qn} from (7) and (8) can be substituted into (6) to yield

$$I_{sn} = \frac{-V_{sn} \sin \gamma}{\omega_n L_{qn} \cos \gamma} \quad (9)$$

This expression (9) can then be substituted into (5) and rearranged as follows,

$$V_{sn} (L_{qn} - L_{dn}) \cos^2 \gamma + \omega_n \Psi_{mn} L_{qn} \cos \gamma + V_{sn} L_{dn} = 0 \quad (10)$$

Two new variables are defined as follows:

$$\zeta = \frac{L_{qn}}{L_{dn}} \quad (11)$$

$$\alpha = \frac{\omega_n \Psi_{mn}}{V_{sn}} \quad (12)$$

Equation (10) can be rewritten using (11) and (12) in a more compact form as follows:

$$(\zeta - 1) \cos^2 \gamma + \alpha \zeta \cos \gamma + 1 = 0 \quad (13)$$

Equation (13) can be readily solved to yield

$$\cos \gamma = \frac{-\alpha \zeta + \sqrt{(\alpha \zeta)^2 - 4(\zeta - 1)}}{2(\zeta - 1)} \quad (14)$$

Manipulation of (9) and (14) leads to the interesting result as follows,

$$\lim_{\alpha \rightarrow \infty} I_{sn} = \frac{\Psi_{mn}}{L_{dn}} \quad (15)$$

Therefore, according to equation (12) and (15), it's found that the current of the motor trends to a constant

value determined by flux and d-axis inductance, as α increases.

3.3 Effect of battery capacity on UCG

The other simulation was implemented with 0.5Ah battery capacity. And the results of this simulation are shown in Figure 11. Compared to Figure 7, the battery current is smaller, while the terminal voltage of the battery is higher. The reason is the battery internal resistance will increase correspondingly when the battery capacity decreases, which is determined by the characteristics of the battery. Meanwhile, although the current decreases, the battery capacity decreases more. Therefore, the SOC of battery gets more increment.

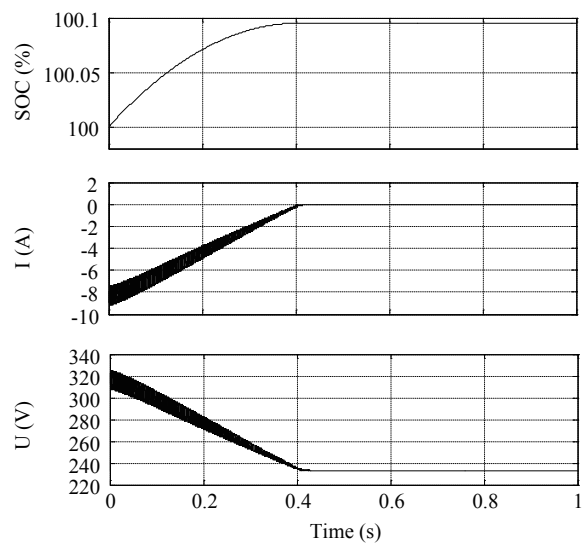


Fig. 11 SOC, current and output voltage of battery under capacity of 0.5 Ah

3.4 The leakage resistances

Tobishima [Tobishima and Yamaki, 1999] shown charging battery experiments with different charge rate. Cells overcharged by more than 2 C caught fire after the rapid cell temperature increase caused by electrolyte decomposition. The charging current of the battery is high, even greater than 2 C, as shown in our simulation results. Therefore, the leakage resistances are assigned to the circuit to avoid overcharge of the battery. The battery is disconnected when the UCG occurs and the discharge resistances are connected to DC side of the rectifier.

Figures 12, 13 and 14 shows the biggest resistance brings a high voltage, while the smallest one leads to longest time of UCG. Therefore the optimized resistance is needed.

4. CONCLUSION

This paper developed a simple analytical model of UCG, and then the transient simulations of UCG proc-

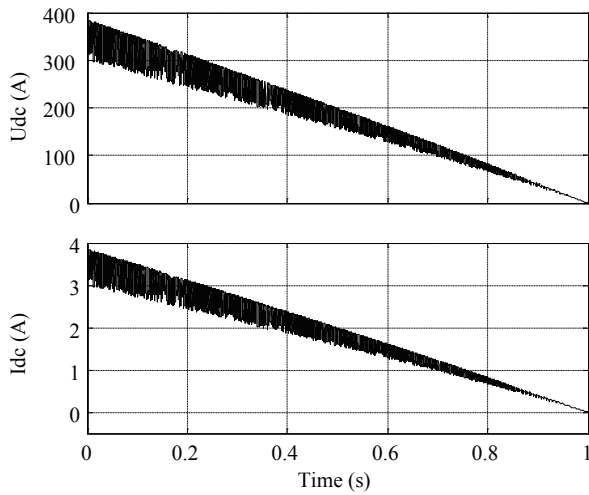


Fig. 12 Voltage and current on 100 Ω resistance

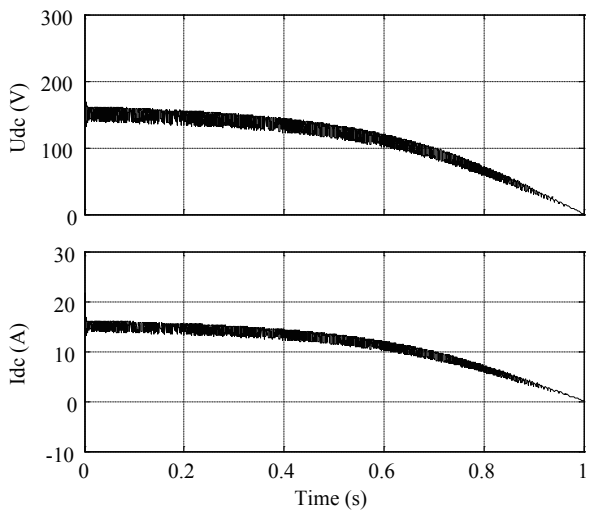


Fig. 13 Voltage and current on 10 Ω resistance

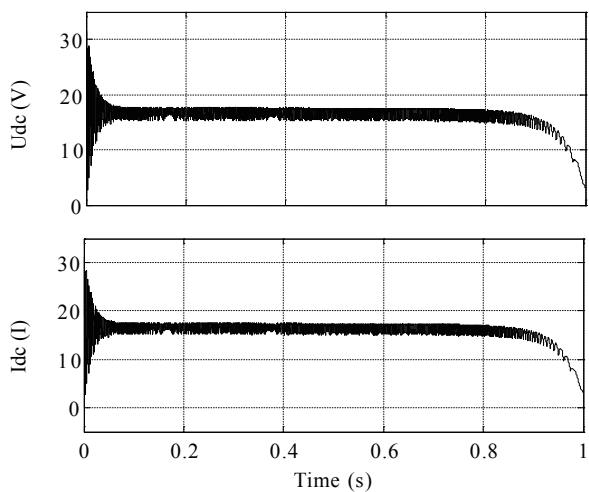


Fig. 14 Voltage and current on 1 Ω resistance

ess were implemented. Different motor speeds and battery capacities were applied in the simulations. Meanwhile, the absorbed energy of the battery was estimated. Furthermore, in order to avoid the breakdown risk of the battery, inverter, motor and other relevant components, the leakage resistances were assigned to the circuit. This research could be used to understand the UCG process and improve the electrical power-train system performance in the hybrid vehicles.

REFERENCES

Adnanes, A. K., R. Nilssen, R. O. Rad, Power feedback during controller failure in inverter fed permanent magnet synchronous motor drives with flux weakening, *Proceedings of Power Electronics Specialists Conference*, Vol. 2, 958-963, 1992.

Bianchi, N., S. Bolognani, and M. Zigliotto, Analysis of PM synchronous motor drive failures during flux weakening operation, *Proceedings of Power Electronics Specialists Conference*, Vol. 2, 1542-1548, 1996.

Jahns, T. M., and V. Caliskan, Uncontrolled generator operation of interior PM synchronous machines following high-speed inverter shutdown, *IEEE Transactions on Industry Applications*, Vol. 35, No. 6, 1347-1357, 1999.

Kassakian, J. G., Automotive electrical systems-the power electronics market of the future, *Proceedings of APEC 2000*, Vol. 1, 3-9, 2000.

Liaw, C. Z., D. M. Whaley, W. L. Soong, N. Ertugrul, Investigation of inverterless control of interior permanent-magnet alternators, *IEEE Transactions on Industry Applications*, Vol. 42, No. 2, 536-544, 2000.

Liaw, C. Z., W. L. Soong, B. A. Welchko, N. Ertugrul, Uncontrolled generation in interior permanent-magnet Machines, *IEEE Transactions on Industry Applications*, Vol. 41, No. 4, 945-954, 2005.

Soong, W. L. and N. Ertugrul, Inverterless high-power interior permanent-magnet automotive alternator, *IEEE Transactions on Industry Applications*, Vol. 40, No. 4, 1083- 1091, 2004.

Tobishima, S, and J. Yamaki, A considerat ion of lithium cell safety, *Journal of Power Sources*, Vol. 81-82, 882-886, 1999.

(Received March 4, 2011; accepted March 8, 2011)